9854 *Macromolecules* **2010**, *43*, 9854–9858
DOI: 10.1021/ma101704k

Macromolecules
ARTICLE

Macromolecular Orientation in Glassy Starch Materials That Exhibit Shape Memory Behavior

Cyril Véchambre,[†] Alain Buléon,[†] Laurent Chaunier,[†] Frédéric Jamme,[‡] and Denis Lourdin*[,†]

[†]*INRA, UR1268, Unité Biopolymères Interactions et Assemblages, 44300 Nantes, France, and*
[‡]*Synchrotron Soleil, L'orme des merisiers, 91192 Gif-sur-Yvette, France*

Received July 28, 2010; Revised Manuscript Received October 8, 2010

ABSTRACT: This paper explores the molecular mechanisms involved in residual stress in relation with shape memory effects in glassy amorphous starch. Wide-angle X-ray scattering (WAXS) and synchrotron radiation (SR) polarized infrared microspectroscopy were used to analyze the structural anisotropy revealed by polarized light microscopy. A local molecular orientation was evidenced by WAXS and IR dichroism. Results clearly demonstrate that the residual stress observed in the temporary shape is due to local molecular orientation in amorphous starch resulting from the flow of matter induced by the deformation process. The molecular orientation disappears when the sample relaxes and recovers its initial shape.

Introduction

Beginning with the pioneering works of Kovacs (1958),[1] shape memory effects in polymers have been widely studied for designing new "smart materials" and actuators.[2−4] Since then, and despite numerous studies, the mechanisms involved in shape memory polymers (SMP) are not yet completely elucidated. SMP have the capability to recover their original shape after being deformed into a temporary shape. In the case of thermoplastic SMP,[5] the shape memory effect is usually attributed to the presence of two types of domain: one flexible and one rigid. The rigid domains determine the initial shape while the more flexible domains become oriented in the temporary shape. This orientation remains stable below the glass transition temperature "T_g". However, once the temperature goes above T_g, these domains relax and lead to the recovery of the initial macroscopic shape of the sample.

The observation of molecular orientation in polymers by X-ray diffraction as well as spectroscopic techniques has been the subject of prior research.[6−8]

Starch is the major energy reserve of a wide variety of higher plants such as cereals, legumes, and tubers. As an abundant and inexpensive renewable resource, it is increasingly utilized in the manufacture of biodegradable or biocompatible materials. Starch is biosynthesized as semicrystalline granules containing two polymers of glucose, the linear amylose and the highly branched amylopectin.[9] Most starch-based materials are derived from hydrothermal processing and melting disruption of the native starch structure, once starch granules are disrupted the material properties strongly depend on the way amylose and amylopectin reorganize.[10] Thus, after being mixed with water and other molecules such as glycerol or sorbitol,[11,12] starch can be processed into thermoplastic material by extrusion,[13] water acting as plasticizer during extrusion. We have demonstrated that extruded thermoplastic starch can present the shape memory effect.[14,15] The hydrophilic property of starch can be used to trigger the shape recovery. Extruded thermoplastic starch materials present very efficient shape-memory capabilities, with a high recovery ratio, $R_r > 90\%$, for a deformation ratio of 200%, similar to that of synthetic SMP such as semicrystalline polyurethane (PU) or biopolymer-based smart materials such as polylactide-*co*-poly(glycolide-*co*-caprolactone) (PLAGC). The starch shape memory effect has been shown to originate from the amorphous state, and recrystallization, even partial, reduces its efficiency.[15] At the macroscopic scale, it is related to residual stresses stored in the temporary shape, leading to specific birefringence under polarized light. The shape recovery corresponds to the relaxation of such residual stresses at temperatures close to the glass transition.[15]

The major aim of this study is to investigate the existing relationship between these types of residual stress and macromolecular orientation induced into the temporary shape by process deformation. Residual stress containing areas were first evidenced using polarized light microscopy. Synchrotron polarized infrared microspectroscopy was used for the first time to detect local macromolecular orientation on biopolymer-based materials. It allowed to work at resolution not exceeding 12 μm and with reduced recording time due to very high brilliance. WAXS (wide-angle X-ray scattering) is a more usual technique to detect orientation especially in semicrystalline materials. It could also be used on amorphous polymers using azimuthal integration of the amorphous scattering band.[6]

Experimental Section

Raw Material. Native potato starch was obtained from Roquette (Lestrem, France). The amylose/amylopectine ratio was 23/77.

Extrusion. Starch was mixed with water and glycerol prior to extrusion. The moisture content was set at 26% wet basis (wb), and the amount of glycerol was adjusted to 10% wb. The mixture was extruded under usual conditions (T_{die}: 115 °C; die pressure: 130 bar; torque: 16 N m) using a SCAMIA single-screw device (Rheoscam Type 20.11d, Crosne, France). Special care was taken to set a low screw speed (20 rpm) in order to avoid the macromolecular orientation due to flow at the extruder outlet. Flat ribbons with a 25 mm width and a thickness of 5 mm were obtained. They were stored in closed vessel at a stable relative humidity (RH = 59%) using a saturated salt solution of sodium bromide at 20 °C under a partial vacuum for 15 days.

*Corresponding author: Tel +33 (0)2 40 67 51 47; Fax +33 (0)2 40 67 50 43; e-mail denis.lourdin@nantes.inra.fr.

 Published on Web 11/12/2010

Table 1. Indication about Glass Transition, Deformation Temperature, and Deformation Ratio for the Longitudinal and the Transversal Samples

specimen	glass transition temperature (T_g, °C)	deformation temperature (T_d, °C)	deformation ratio (D_r, %)
longitudinal sample	50	50	100
transversal sample	50	80	400

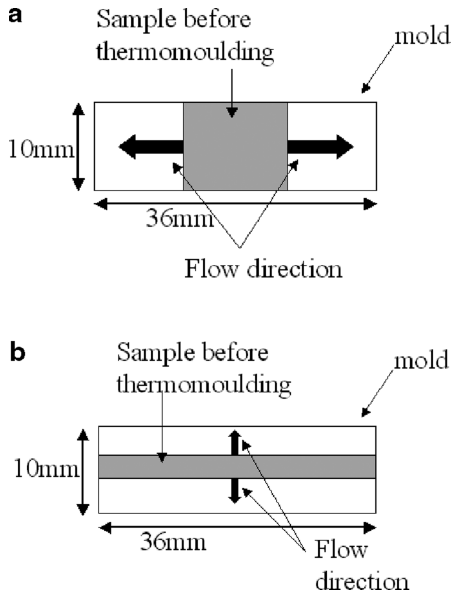

Figure 1. Schematic representation of the melt flow during the thermomolding process for (a) longitudinal and (b) transversal samples.

After sorption equilibrium, flat ribbons presented a final water content of 12% wb.

Thermomolding. Two types of constrained samples were prepared, depending on the melt flow direction during thermomolding in the rectangular mold used (Table 1). The first type called "longitudinal" corresponds to a flow parallel to the length of the mold (Figure 1a) contrary to the "transversal" type for whom the flow was perpendicular to the length of the mold (Figure 1b).

To prepare the longitudinal samples, ribbons of 18 mm long by 10 mm wide were cut and arranged in the center of a rectangular (36 × 10 mm) and airtight mold and heated at a deformation temperature (T_d) of 50 °C. A pressure of 200 bar was applied to the sample that flowed along the longitudinal direction into the mold. The final sample dimensions were $36 \times 10 \times 2.5\ mm^3$ ($l \times w \times t$). The corresponding deformation ratio, D_r, was 100%. The resulting barrels were then cooled to ambient temperature and equilibrated at RH = 59% for 5 days.

Transversal samples were prepared from ribbons 36 mm long by 2 mm wide, heated in the center of the mold to T_d 80 °C, the temperature required to achieve high level of deformation. A pressure of 200 bar was applied to the sample that flowed along the radial direction into the mold. The final sample dimensions were $36 \times 10 \times 0.32\ mm^3$ ($l \times w \times t$), which corresponded to a D_r of 400%. The resulting barrels were then cooled to ambient temperature and equilibrated at RH = 59% for 5 days.

A low heat rate of 3 °C/min was chosen in order to limit the temperature gradient in the sample. When T_d was reached, the pressure was applied gradually.

The extruded ribbon before thermomolding was considered as an isotropic "reference sample" without birefringence. It was named unconstrained sample. This sample did not exhibit any shape memory properties.

Shape Recovery. Constrained samples were placed in a high relative humidity atmosphere (RH = 100%) for 8 h in order to make them to relax and recover their original shape. The resulting samples were called relaxed samples. After recovery they were stored at a relative humidity of 59%.

Water Content and Glass Transition Measurement. The water content of the samples was measured by thermogravimetric analysis using a TGA2050 (T.A. Instruments, New Castle, DE). It was evaluated for ~10 mg of bulk sample maintained at 130 °C for 90 min. The glass transition was determined by differential scanning calorimetry (DSC) using a T.A. Q100 instrument (T.A. Instruments, New Castle, DE). The system was calibrated with indium, and ~10 mg of bulk sample was placed in sealed stainless-steel cells. Two successive scans were run at 3 °C/min between 0 and 160 °C, separated by a cooling stage. The glass transition temperature was determined on the second scan at the midpoint of the calorific capacity change on the thermogram.

Polarized Light Microscopy. Birefringence linked to the residual stress was observed using a modular stereomicroscope, Leica MZ 12-5 (Wetzlar, Germany), with a polarized light device at a magnification of 10×.

Wide-Angle X-ray Scattering (WAXS). Two-dimensional WAXS diagrams were recorded from starch barrels using a Bruker D8 X-ray diffractometer (Madison, WI) equipped with a two-dimensional GADDS detector. The X-ray radiation, Cu $K\alpha_1$ (λ = 0.154 05 nm), produced in a sealed tube at 40 kV and 40 mA was selected and parallelized using a Gobël mirror parallel optics system and collimated to produce a 500 μm beam diameter. WAXS diagrams were recorded in the transmission mode with specimens lying with their length parallel to the vertical axis of the detector. Orientation was determined by azimuthal integration between 0.680 and 0.386 nm corresponding to the amorphous scattering band. Background as well as beamstop profiles were subtracted from the sample signals; the resulting signal was smoothed for more clarity. Recording time was 20 min.

Synchrotron Infrared Microspectroscopy. All spectra were recorded in reflection mode on a Continuμm XL microscope (Thermo Scientific), coupled to a Nicolet 5700 FTIR spectrometer (Thermo Scientific). The microscope was equipped with a 32X Schwarzschild objective (numerical aperture (NA): 0.65), with a 50 μm liquid nitrogen cooled MCT detector. The experiments were carried out at the SMIS beamline of the SOLEIL Synchrotron (Gif sur Yvette, France).[16] The IR source was produced by the broadband synchrotron infrared radiation from a bending magnet. A highly polarized (referred to as the parallel direction) bright beam was available at the focal plane of the microscope.

The microscope operates in confocal mode, using a 32× infinity corrected objective (NA: 0.65). All spectra were collected using a double path single masking aperture size of $12 \times 12\ \mu m^2$. Individual spectra were saved in $\log(1/R)$ format at 8 cm^{-1} spectral resolution, with 128 coadded scans. Data acquisition and Kramers−Kronig transformations were performed using Omnic software (Version 7.4, Thermo Scientific, Waltham, MA).

IR mapping was performed on unconstrained, constrained (longitudinal and transversal), and relaxed samples using dïchroism. The polarization vector of the beam was parallel to the length of the sample for the spectra recorded in mode parallel while for the spectra recorded in mode perpendicular the polarization vector of the beam was perpendicular to the length of the sample. The original spectra were preprocessed by multiplicative signal correction (MSC) using the Unscrambler v 9.8 (Camo, Oslo, Norway) to avoid a physical light-scattering effect. After MSC, the data were then analyzed by principal component analysis (PCA) using the Unscrambler software. All experiments were realized in different area of the specimen in order to check the sample homogeneity.

Results

The samples stored at a relative humidity of 59% had a water content of 12% wet basis (wb) and a glass transition of 50 °C.

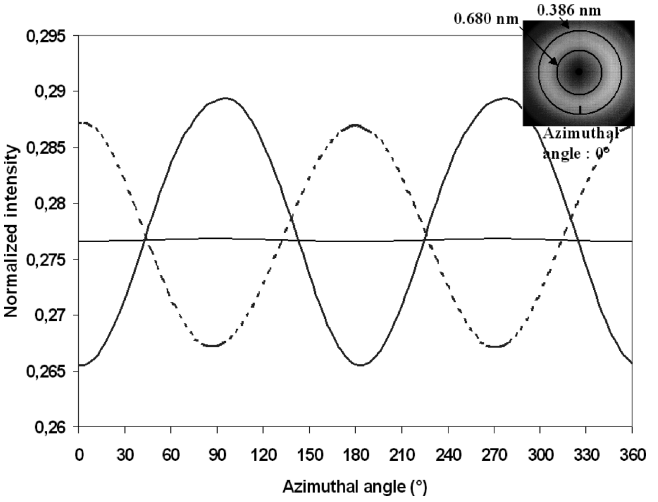

Figure 2. Orientation diagrams from WAXS spectra. Bold full line represents the azimuthal scan of the longitudinal sample, dotted line represents the azimuthal scan of the transversal sample, and full line represents the relaxed sample.

In polarized light microscopy, constrained samples (extrusion followed by thermomolding) show typical and clearly visible birefringence fringes, contrary to unconstrained samples (extrusion without thermomolding), which do not present any specific birefringence. This observation evidence the presence of anisotropy in the constrained samples which originates from residual stress. It was checked that the birefringence fringes disappear after recovery.[14]

WAXS diagrams present no clear diffraction peak but only a broad amorphous scattering band. The scattering band maximum corresponds to a repeat distance of about 0.5 nm. This is normally considered to arise from the van der Waals contact of nonbonded atoms (VDW spacings).[7] Figure 2 represents the azimuthal integration of the scattering intensity between 0.680 and 0.386 nm for the longitudinal, the transversal, and the relaxed samples.

Constrained samples exhibit periodic scattering intensity changes with the azimuthal angle. For the longitudinal samples the maximum intensity, observed at 90° and 270°, shows that orientation is parallel to the length of the specimen. While for the transversal samples the maximum intensity observed at 0°, 180°, and 360° corresponds to a perpendicular orientation to the length of the specimen. No periodic scattering intensity was observed for the relaxed samples as for unconstrained samples (data not shown). These results confirm that thermomolding induces an orientation of the amorphous phase in the direction of the melt flow. Such orientation is stable while moisture contents maintains the sample in the glassy state (below T_g). This orientation disappears during shape recovery.

The water content has a strong influence on the properties of starch. It creates intramolecular bonds that are implicated in the possibilities of the macromolecules to stretch. Then, the water content was sharply maintained constant, at 12% (wb), during analysis.

Polarized infrared spectroscopy provides information about molecular orientation in anisotropic samples using the difference between absorption spectra recorded using a parallel (PAR) or perpendicular (PER) polarized infrared beam (dichroism). Figure 3a shows a typical average spectrum of a series of IR spectra recorded in the parallel and perpendicular mode from "longitudinal" constrained samples.

Weak but significant differences are observed between PAR and PER spectra, contrary to unconstrained samples (spectra not shown), which confirm the presence of a specific orientation in

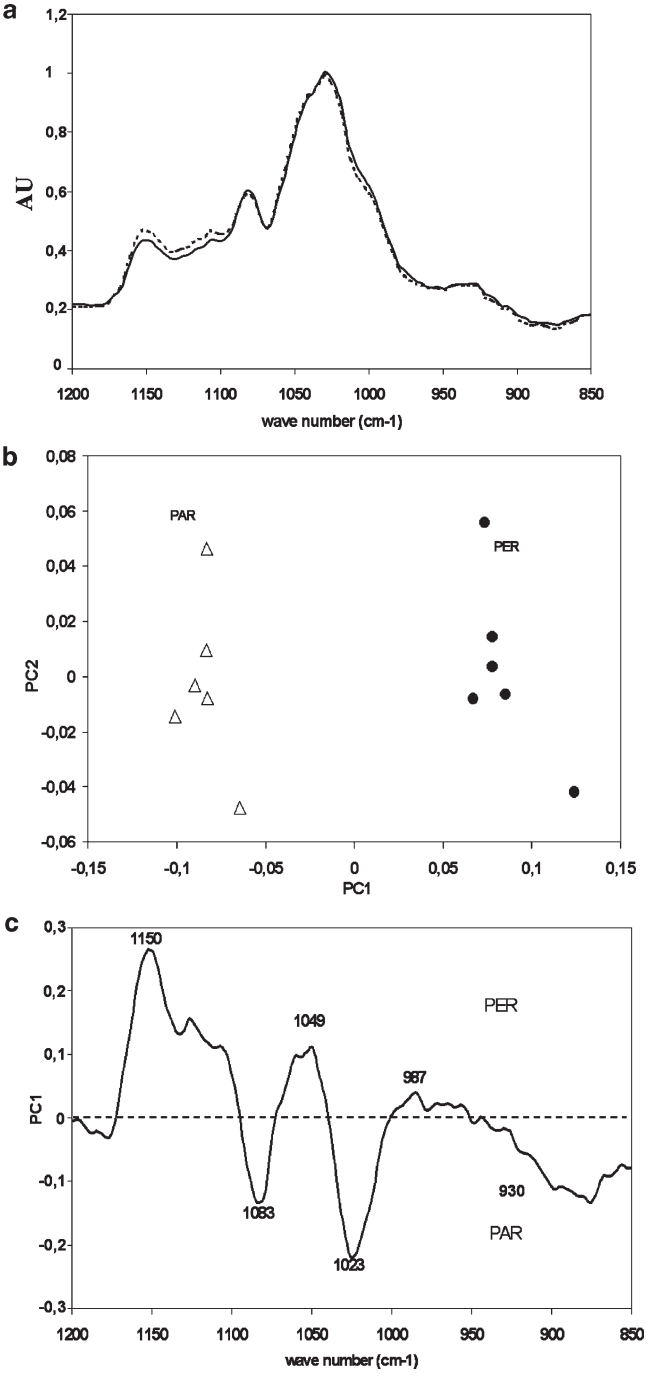

Figure 3. SR infrared microspectroscopy of a longitudinal sample: (a) average spectrum of a collection of infrared spectra recorded with polarization parallel (full line) and perpendicular (dotted line) to the length of the sample; (b) PCA score of IR spectra (triangle for parallel spectra and circles for perpendicular spectra); and (c) first principal component loading vector determined by the PCA.

the constrained samples. To enhance the main variation in the data sets and to analyze the correlation of the main FT-IR absorbance bands with orientation in the wavelength domain (1200−850 cm^{-1}), data were analyzed by principal component analysis (PCA). The spectra recorded in the parallel and the perpendicular modes are clearly different for constrained samples and unconstrained samples. In the case of the constrained "longitudinal" samples, the first principal component, which accounts for 81% (PC1) of the total variation in the data set (Figure 3b), clearly allows differentiation between the two types of spectra.

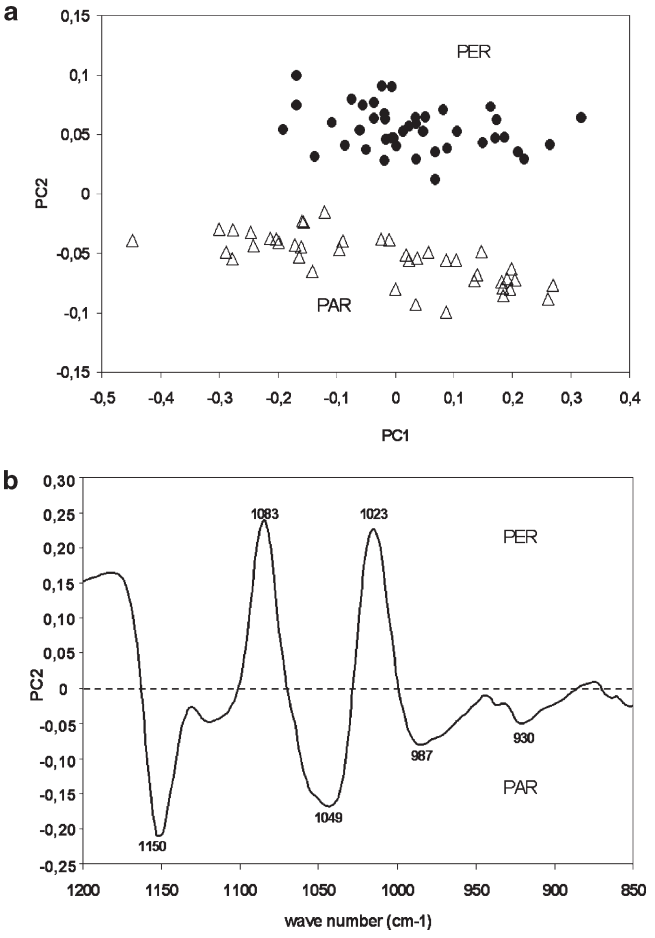

Figure 4. PCA analysis of IR spectra recorded from a transversal sample: (a) PCA score (triangle for parallel spectra and circles for perpendicular spectra) and (b) second principal component loading vector.

This difference between parallel and perpendicular absorbance for the longitudinal samples confirms their structural anisotropy also observed in polarized light microscopy and X-ray scattering. The corresponding loading plot (Figure 3c) exhibits specific vibration frequencies; PAR spectra are mainly characterized by peaks at 1083 and 1023 cm^{-1} and negative scores with regard to PC1, while major peaks are present at 1150, 1049, and 987 cm^{-1} in the PER spectra, with positive scores of PC1.

The same technique was used on "transversal" samples that have an orthogonal orientation to the "longitudinal" samples as determined by X-ray scattering. The resulting PCA also clearly differentiates PAR spectra from PER spectra (Figure 4a), but the principal component involved in the discrimination is in that case the second vector which accounts for 20% of the total variation in the data set.

In the corresponding loading plot (Figure 4b) peaks at 1083 and 1023 cm^{-1} are predominant for PER spectra with positive scores of PC2, while PAR spectra are characterized by peaks at 1150, 1049, and 987 cm^{-1} and negative scores of PC2.

Considering the melt flow direction during thermomolding, PAR spectra for longitudinal samples and PER spectra for transversal samples both correspond to spectra recorded with a beam parallel to the flow direction. As the two series of spectra are characterized by the same peaks at 1083 and 1023 cm^{-1} in the loading plots, one can conclude that these absorption frequencies are linked to molecular orientation.

PCA score of relaxed samples (Figure 5) shows no difference between PAR and PER spectra which confirm that no specific orientation is present after shape recovery.

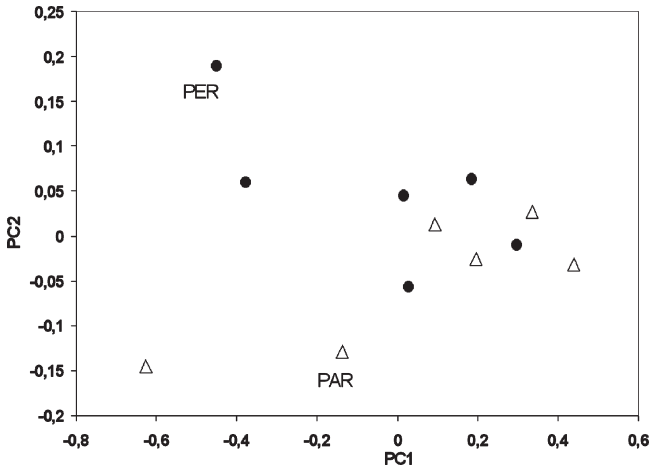

Figure 5. PCA score of IR spectra recorded from the relaxed samples (triangle for parallel spectra and circles for perpendicular spectra).

Discussion

In the frequency domain ranging from 1200 to 850 cm^{-1}, the C−C, C−O, C−H stretching, and C−O−H bending of starch are observed.[17,18] The relative intensity of corresponding bands or groups of bands has been assigned to starch modification such as retrogradation,[18−20] amorphous relaxation,[21] or crystallization.[22−24] This was also used for studying the influence of the water content on the structure of native starch.[22,25] According to Fang and co-workers,[26] the bands located at 1023 and 1083 cm^{-1} could be assigned to the C−O bond stretching in the C−O−C group of the anhydroglucose rings. The peak at 1023 cm^{-1} has been shown to be typical of amorphous starch while that at 1049 cm^{-1} develops with crystallinity. Therefore, the intensity of these two peaks has been widely used to determine the amount of ordered starch to amorphous starch.[20,22,24] The band at 987 cm^{-1} is very sensitive to hydration and can shift from 987 to 1003 cm^{-1} depending on the water content.[22] The value observed here is in agreement with the very small hydration level of the samples. It was attributed to intramolecular hydrogen bonding of the hydroxyl group at C-6.[22] It was also shown to develop with molecular ordering.[24,25,27] The band at 1153 cm^{-1} was assigned by Bernazzani and co-workers[27] to vibrations in the environment of ordered single helices. In the same study, bands at 1126, 1101, and 999 cm^{-1}, which are also present in the loading plots with the more intense bands at 1150 and 1049 cm^{-1}, were shown to increase with increasing annealing temperature and increasing order.

When looking at the loading plots (Figures 3b and 4b), the main bands typical of amorphous starch correspond to the PAR spectra obtained on longitudinal samples and the PER spectra obtained on the transversal ones and therefore to spectra recorded when the polarization is parallel to the orientation. On the contrary, all the bands assigned to higher order and/or crystallinity are linked to spectra recorded when the polarization is perpendicular to the direction of the orientation; it shows that local orientation is more present in amorphous domains and is limited by ordered domains. The clear presence of orientation in amorphous starch may be surprising and could, in fact, only be due to very local ordering and paracrystallinity without real crystalline packing. This is in agreement with the WAXS results. The 987 cm^{-1} band can be linked to both hydrogen bonding and order. Here, it appears with the band characteristic of order and its location at 987 cm^{-1} clearly confirm that the studied samples were not highly hydrated. The band at 930 cm^{-1}, which has been assigned to skeletal mode involving in α(1−4) linkage,[17] is linked to the orientation of the longitudinal samples, while for the

transversal samples the same band can be more linked to the order. This result is surprising and could be due to a larger size of oriented domains in the longitudinal samples.

Figure 2 shows that the normalized scattering intensity is slightly higher for the longitudinal samples. This means that the longitudinal samples could be a slightly more oriented. This is in agreement with the results of the PCA performed on the IR spectra, the weight associated with the component linked to orientation being 81% and 20% for longitudinal and transversal samples, respectively. This difference can be linked to the different ratio of shape recovery for the 2 samples (5% higher for the longitudinal sample) and explained by the different temperature used for their thermomolding.[15] A deformation temperature of 80 °C was applied to the transversal samples in order to reach a deformation ratio of 400%. At this temperature the macromolecules have enough energy to reorganize between the end of the deformation process and the freezing of the structure, in contrast to the longitudinal samples which were deformed at a lower temperature closer to their T_g.

Recent studies[28,29] have shown the orientation of soft segments in the temporary shape of SMPs. Our results, and especially the original use of SR infrared microspectroscopy, indicate a similar molecular orientation in shape memory starch. SR polarized IR microspectroscopy was used for the first time on biopolymeric materials. This allowed confirming the presence of orientation as detected by WAXS with a much higher resolution (12 μm). It mainly contributes to show that amorphous domains are mainly involved in the shape memory effect but also that some ordered domains are present within the samples. The presence of bands linked to hydrogen bonds and α(1−4)linkage could evidence the presence of local order under the form of helical fragments which may be stabilized by intramolecular H bonds.[27] This results from the deformation imposed by mechanical pressure during the heating and cooling stages of the thermomolding process.

Conclusion

Local orientation and local order were studied in shape memory starch materials. It has been shown that glassy starch in the temporary form contains residual stresses. As shown by WAXS and SR infrared spectroscopy, their stresses are linked to local molecular orientation induced by the deformation process. Orientation as well as residual stresses remain stable in the glassy state. They are at the root of the shape recovery, which occurs when the temperature rises above T_g as a result of moisture uptake or heating. In analogy to the commonly referred shape memory effect, it appears that the amorphous phase could coincide with the flexible domains, while the ordered phase would correspond to rigid domains. No crystallinity was detected by WAXS, indicating that only local order was present. Moreover, the SR polarized infrared spectroscopy showed that local orientation was greater in the amorphous domains.

Acknowledgment. This study was carried out with the support of the French Environment and Energy Management Agency (ADEME) as well as the INRA/CNRS CPDD programs. The authors thank R. Désirest and B. Pontoire (INRA, Nantes) for extrusion experiments and X-ray diffraction analysis as well as P. Robert (INRA, Nantes) and P. Dumas (SOLEIL, French synchrotron facility) for helpful discussions.

References and Notes

(1) Kovacs, A. J. *J. Polym. Sci.* **1958**, *30*, 131–147.
(2) Lendlein, A.; Kelch, S. *Angew. Chem., Int. Ed.* **2002**, *41*, 2034–2057.
(3) Behl, M.; Lendlein, A. *Mater. Today* **2007**, *10*, 20–28.
(4) Liu, C.; Qin, H.; Mather, P. T. *J. Mater. Chem.* **2007**, *17*, 1543–1558.
(5) Wang, Y. L.; Li, Y. G.; Luo, Y. F.; Huang, M. N.; Liang, Z. Q. *Mater. Lett.* **2009**, *63*, 347–349.
(6) Pick, M.; Lovell, R.; Windle, A. H. *Polymer* **1980**, *21*, 1017–1024.
(7) Miller, R. L.; Boyer, R. F.; Heijboer, J. *J. Polym. Sci., Part B: Polym. Phys.* **1984**, *22*, 2021–2041.
(8) Ward, I. M. *Adv. Polym. Sci.* **1985**, *66*, 81–115.
(9) Buléon, A.; Colonna, P.; Planchot, V.; Ball, S. *Int. J. Biol. Macromol.* **1998**, *23*, 85–112.
(10) Colonna, P.; Buléon, A. In *Starch: Characterization, Properties and Applications*; Bertolini, A., Ed.; CRC Press LLC: Boca Raton, FL, 2009; Chapter 4.
(11) Bizot, H.; LeBail, P.; Leroux, B.; Davy, J.; Roger, P.; Buléon, A. *Carbohydr. Polym.* **1997**, *32*, 33–50.
(12) Lourdin, D.; Coignard, L.; Bizot, H.; Colonna, P. *Polymer* **1997**, *38*, 5401–5406.
(13) DellaValle, G.; Boche, Y.; Colonna, P.; Vergnes, B. *Carbohydr. Polym.* **1995**, *28*, 255–264.
(14) Chaunier, L.; Lourdin, D. *Starch/Staerke* **2009**, *61*, 116–118.
(15) Véchambre, C.; Chaunier, L.; Lourdin, D. *Macromol. Mater. Eng.* **2010**, *295*, 115–122.
(16) Polack, F.; Mercier, R.; Nahon, L.; Armellin, C.; Marx, J. P.; Tanguy, M.; Couprie, M. E.; Dumas, P. *Proc. SPIE Accel.-Based Sources Infrared Spectrosc. Appl.* **1999**, *3775*, 13−21.
(17) Cael, J. J.; Koenig, J. L.; Blackwell, J. *Biopolymers* **1975**, *14*, 1885–1903.
(18) Goodfellow, B. J.; Wilson, R. H. *Biopolymers* **1990**, *30*, 1183–1189.
(19) Wilson, R. H.; Goodfellow, B. J.; Belton, P. S.; Osborne, B. G.; Oliver, G.; Russell, P. L. *J. Sci. Food Agric.* **1991**, *54*, 471–483.
(20) Smits, A. L. M.; Ruhnau, F. C.; Vliegenthart, J. F. G.; Van Soest, J. J. G. *Staerke* **1998**, *50*, 478–483.
(21) Willett, J. L. *Macromol. Chem. Phys.* **2008**, *209*, 764–772.
(22) Van soest, J. J. G.; Tournois, H.; Dewit, D.; Vliegenthart, J. F. G. *Carbohydr. Res.* **1995**, *279*, 201–214.
(23) Rindlav, A.; Hulleman, S. H. D.; Gatenholm, P. *Carbohydr. Polym.* **1997**, *34*, 25–30.
(24) Sevenou, O.; Hill, S. E.; Farhat, I. A.; Mitchell, J. R. *Int. J. Biol. Macromol.* **2002**, *31*, 79–85.
(25) Capron, I.; Robert, P.; Colonna, P.; Brogly, M.; Planchot, V. *Carbohydr. Polym.* **2007**, *68*, 249–259.
(26) Fang, J. M.; Fowler, P. A.; Tomkinson, J.; Hill, C. A. S. *Carbohydr. Polym.* **2002**, *47*, 245–252.
(27) Bernazzani, P.; Chapados, C.; Delmas, G. *J. Polym. Sci., Part B: Polym. Phys.* **2000**, *38*, 1662–1677.
(28) Wong, Y. S.; Venkatraman, S. S. *Acta Mater.* **2010**, *58*, 49–58.
(29) Therien-Aubin, H.; Gautrot, J. E.; Zhang, J.; Zhu, X. X. *Polymer* **2010**, *51*, 22–25.